J Therm Spray Tech (2018) 27:1551–1562
https://doi.org/10.1007/s11666-018-0769-0

PEER REVIEWED

Low-Temperature Transformation of Amorphous Sol–Gel TiO_2 Powder to Anatase During Cold Spray Deposition

Agnieszka Baszczuk[1] · **Marek Jasiorski**[1] · **Marcin Winnicki**[2]

Submitted: 15 April 2018 / in revised form: 12 September 2018 / Published online: 10 October 2018

Abstract Nanocrystalline TiO_2 coatings were successfully deposited on metallic substrate surfaces through low-pressure cold spray. Sol–gel amorphous TiO_2 dry gel was for the first time used as a feedstock powder. Agglomerated morphology of the amorphous powder with high-density packing of particles and reduced pores number was an important factor for successful low-pressure cold spraying. However, in the present study one more factor contributing to anchoring of TiO_2 particles by cold gas spraying onto a substrate was indicated. This factor enabling effective powder deposition and coating production is based on an exotic for conventional ceramic materials' plastic deformation of amorphous powder. Furthermore, the detailed analysis of SEM, Raman and XRD measurements clearly demonstrated that amorphous titanium dioxide is transformed into crystalline anatase form during the process of low-pressure cold spraying.

✉ Agnieszka Baszczuk
agnieszka.baszczuk@pwr.wroc.pl;
agnieszka.baszczuk@pwr.edu.pl

Marek Jasiorski
marek.jasiorski@pwr.edu.pl

Marcin Winnicki
marcin.winnicki@pwr.edu.pl

[1] Department of Mechanics, Materials Science and Engineering, Wroclaw University of Science and Technology, Smoluchowskiego 25 Str., 50370 Wrocław, Poland

[2] Department of Materials Science, Strength and Welding Technology, Wroclaw University of Science and Technology, Łukasiewicza 5 Str., 50371 Wrocław, Poland

Keywords ceramic low-pressure cold spray coatings · low-pressure cold spray · sol–gel · titanium dioxide deposition

Introduction

Titanium dioxide has been the most investigated metal oxide because of diversity of its applications for instance in electrochromic devices, photocatalytic converters, gas sensors or solar cells (Ref 1). TiO_2 is a nontoxic, inexpensive and chemically stable substance. The most promising characteristic of TiO_2 lies in its high photochemical activity. Therefore, titanium dioxide coatings have been attracting researchers' attention concerning their practical applications to environmental cleaning (Ref 2). It is well known that among polymorphous forms (rutile, anatase and brookite), anatase with the forbidden band width $\sim$ 3.1 eV has the highest photochemical activity (Ref 3-5). However, anatase is a thermodynamically metastable polymorph, and irreversible phase transition from anatase to rutile usually occurs with increasing temperature causing the difficulty in producing an extremely active, phase-pure anatase photocatalyst. Therefore, it is a fundamental challenge to find a method of anatase coatings production, preventing at the same time conversion to rutile. Various techniques were developed to deposit ceramic films with desired structural properties including, for example, vapor deposition, electrophoretic deposition, sol–gel or thermal spraying (Ref 6).

Thermal spraying stands out by the fact that it can provide thick coatings over a large area at high deposition rate as compared to other coating processes. Nevertheless, during the traditional thermal spraying, the powder feedstock is melted. As a result the anatase transformation to

rutile is clearly observed in sprayed coatings (Ref 6). Therefore, it is worth emphasizing that cold spray (abbreviated as CS) is clearly distinguishable from other thermal spraying methods by virtue of the fact that it does not need temperature to build up the coating, because the particles adhere to the substrate due to their plastic deformation in solid state. Conventional ceramics are well known to be hard and brittle at room temperature and ambient pressure. Thus, such mechanism of deposition significantly impedes ceramic deposition, although recent attempts demonstrated that this method is able to deposit homogeneous anatase coatings (Ref 6). In majority of papers, showing the possibility of the TiO_2-thick coating cold spraying, agglomeration of the feedstock powder was recognized as being the most important factor for successful coatings fabrication (Ref 7-10). As an example, the TiO_2 film with a mean thickness of 10-15 μm was deposited by Yang et al. (Ref 7) using anatase particles agglomerated by polyvinyl alcohol binder. Salim et al. (Ref 10) produced crystalline (anatase) TiO_2 powder by hydrolysis of $TiOSO_4$ in distilled water with a small addition of inorganic salt (ammonium sulfate) as a binder. The powder was then post-treated to improve its crystallinity by using two methods: the hydrothermal treatment and annealing at 600 °C. The authors have shown that using agglomerated powders produced in the hydrothermal treatment it was possible to sprayed TiO_2 coating with 150 μm thickness. They assumed that NH_4^+ and SO_4^{2-} ion adsorptions on surface of TiO_2 and post hydrothermal treatment have contributed to the formation of an oriented agglomerated structure in a single crystal axis. They believed that it was the key factor that led to the building-up of the coating. They claimed that agglomerated particles break down on impact onto the substrate due to the nanoporosity induced during their production process. The authors stated also that then, crystals were decoupled, forming unstable newly surfaces, which bonded with their counterparts to develop more stable interfaces, thereby building up the coating (Ref 6, 10). The importance of the oriented agglomeration was further examined by Toibah et al. (Ref 8) which investigated the influence of $(NH_4)_2SO_4$ binder on agglomeration process of TiO_2 and the further properties of the coatings. The authors (Ref 8) observed that adding $(NH_4)_2SO_4$ during the synthesis not only agglomerates the nanoparticles into a micro-sized structure, but also promotes mobility of dislocation to occur when high pressure and temperature were applied during the CS process.

As is known, the agglomeration state can be obtained in two different ways: by using binders or during the sintering operation. In sintered aggregates binding between particles occurs due to chemical diffusion between particles, while in the case of non-sintered soft agglomerates liquid films hold the particles together. Therefore, the interparticle bond energies range from weak liquid bridge forces (soft agglomerates) to stronger solid-state necks (hard agglomerates). This change in the strength of interparticle forces must involve the change in the mechanism responsible for aggregates deposition (Ref 11). The importance of the inherent feedstock structure of the ceramic powder used for CS was very thoroughly analyzed by Vilardell et al. (Ref 11). and Cinca et al. (Ref 12). The authors of these works compared the mechanism of hydroxyapatite (HA) coatings deposition, considering sintered hydroxyapatite particles and non-sintered agglomerated HA. They claimed that the deposition of the sintered HA powders was observed to proceed through pore collapse, fragmentation and densification as well as grain refinement (Ref 12). According to the authors, grain boundaries of initial sintered HA particles are the weak sites, and thus, they easily induce intergranular microcrack formation, behaving as damage initiation points. Damage can further proceed in transgranular mode leading to the formation of small subgrains. On the contrary, in the case of the agglomerated structure of the non-sintered HA powder, the deposition takes place through the compaction of the nanocrystalline grains within the particle upon impact (Ref 11). Rahim et al. (Ref 9) explored the effect of calcination temperatures on TiO_2 feedstock powder prepared by simple hydrolysis method (without the addition of binder and/or inorganic salt) and showed that sintered agglomerated TiO_2 particles, which have less porosity, were difficult to fracture upon impact during the deposition. According to the authors, strong bonds between the particles made them resistant to fragmentation and adherence on surface of the substrate.

It must be additionally recalled that in the 2000s two new ceramic film deposition processes, derived from cold spray process, were developed. These processes are known as an aerosol deposition process (often abbreviated as ADM) and nanoparticle deposition system (often abbreviated as NPDS). In both methods small (submicro- or nano-sized) ceramic particles are sprayed in a vacuum chamber by using a working gas with the pressure below atmospheric (Ref 6, 11). To this day much work has been done to investigate the mechanism responsible for the successful formation and adhesion of solid ceramic coatings by these methods. Generally, in both processes fragmentation and compaction of submicrometer particles into nanoparticles by impact have been reported to be the main bonding mechanism (Ref 11) although the basic physical processes involved in the formation of the coating so far have not been fully clarified (Ref 13).

As it has already been mentioned, the main obstacle to the successful ceramic materials cold spraying is their inherent brittleness, which results from the strong bonding between the metallic and non-metallic elements. Over many consecutive years, various researches were trying to

improve the plasticity of ceramics. At high temperature or under superimposed hydrostatic compression existing deep below the earth's crust or in special testing apparatus, plastic deformation can be achieved in ceramics. However, the maximum achievable deformation is minor even under such severe conditions. Conventional polycrystalline ceramics, such as Al_2O_3, ZrO_2 and TiO_2, are known to be hard and brittle at room temperature and ambient pressure. In contrast to the conventional polycrystalline ceramic materials which are already in use, amorphous oxides (often called soft ceramics) were reported to exhibit remarkable plastic deformation at moderate temperatures (Ref 14-21). The first person to describe the large (non-viscous) plastic deformation in bulk amorphous ZrO_2-Al_2O_3 was in 2003 Gandhi et al. (Ref 14). The authors revealed that bulk amorphous ZrO_2-40 mol.% Al_2O_3 displayed a distinct plastic strain of 15% at 600 °C. They assigned this non-viscous unusual plastic deformation to the open structure of amorphous phase. In 2011 Paul et al. (Ref 15) presented similar behavior in bulk amorphous Al_2O_3-15 mol.% Y_2O_3 sample. The extensive uniaxial deformation of up to 30% was shown by authors for this amorphous mixture. To our knowledge, studies in this field are very scarce (Ref 14-17), and detailed mechanisms and explanations of this deformation are not entirely clear. In 2017 Xu et al. (Ref 17) found that plasticity of amorphous ceramics could be attributed to the metastable state of amorphous phase with free volume and disordered structure. The researchers have demonstrated that the enhanced plastic deformation benefited from higher metastability was mainly resulted from the easier formation and propagation of shear bands. They concluded that ceramic amorphous sample with higher metastability owned larger atomic mobility and local free volume, which was beneficial to the formation of shear bands and further plastic deformation. Accordingly, it is expected that a key parameter responsible for plastic deformation is metastable degree of ceramic material. It is worth noting that formation and propagation of shear bands are also common mechanism inducing plasticity in varieties of metallic and polymeric glasses at temperatures lower than glass transition temperature (T_g) (Ref 22, 23). For these two groups of materials, plasticity can be successfully explained based on free volume theory. This theory was also used by Xu eal. (Ref 17) to clarify plasticity of amorphous solids.

In the light of the considerations set out above, possibility of using agglomerated amorphous titanium dioxide powder for cold spraying seems to be very attractive. It should be stressed that such an alternative feedstock powder has not been used in CS until now. In this work amorphous TiO_2 powder was produced by the sol–gel method. The sol–gel process can be characterized by series of distinct steps (Ref 24, 25). Two first steps of the process (hydrolysis and condensation reactions) in consequence lead to the production of TiO_2 network. When sufficient interconnected network of Ti-O-Ti bonds is formed in a region, colloidal particles in the scale of submicrometer are formed. The alcohol and water released during the hydrolysis and condensation remain in pores of the network, forming colloidal particles. In the next step (called drying) conducted at room temperature, water and other volatile liquids are removed, post-accompanied by further cross-linking and aggregation of particles. The resulting "dry" amorphous powder contains agglomerates created out of the particles linked by electrostatic or van der Waals forces. Uncontrolled room temperature drying and aging do not enable complete removal of organic liquids (e.g., isopropanol). These liquid substances due to their high viscosity are a kind of binders, holding particles together; hence, they have a crucial role in additional stabilization of TiO_2 agglomerates used in this work. The sol–gel method used for oxides production has several advantages over other fabrication methods, for example homogeneity of the products, as a result of homogenous mixing of the starting materials on the molecular level (Ref 26). Nevertheless, gels obtained after sol–gel synthesis are amorphous, not fully condensed, and contain large amounts of organic substances. Transformation of these amorphous gels into a rigid crystalline TiO_2 material requires subsequent calcinations. In this work an attempt to use this drawback, of being amorphous, as a benefit for cold spraying was undertaken. Such possibility of two methods consolidation: low-temperature sol–gel synthesis and cold spraying, seems to be very attractive. In this work sol–gel method to produce amorphous TiO_2 powder which is then used as a feedstock in the process of low-pressure cold spray is used. For the first time it is shown that cold spray process that uses amorphous titania powder as feedstock provides a very convenient way toward fabrication of crystalline anatase coatings. This article identifies cold spray parameters which are necessary for thick TiO_2 coating deposition and for successful crystallization of anatase. Also an attempt for preliminary evaluation of the deposition mechanisms in the case when amorphous TiO_2 particles are used as the feedstock was made.

Experimental Details

Powder Synthesis

Amorphous powder of TiO_2 was self-prepared through a sol–gel method, and the composition was denoted by TiO_2(am), hereafter. The synthesis details were identical to

that described in our previous work (Ref 27). Titanium isopropoxide, isopropanol, deionized water and aqueous ammonia were used as starting materials in the sol–gel synthesis. Their volume ratio was 3:42:7:4, respectively. The prepared solution was stirred in a plastic flask with magnetic stirrer at room temperature in contact with atmospheric oxygen for 2 h. Then the titania colloids were allowed to dry in room temperature yielding final white TiO_2(am) powder.

Substrates Preparation and Design of Spray Process Experiments

Substrate materials were plates of aluminum alloy AA1350 (99.5%) with dimensions of 20 × 20 × 7 mm. The substrates surface was activated by sand blasting under a pressure of 0.6 MPa using alumina sand (mesh 20).

The coatings were sprayed using DYMET 413 (Obninsk Center for Powder Spraying, Obninsk, Russia). The air as a working gas with pressure of 0.5 MPa was used. Spray distance was selected to 10 mm and manipulator traverse speed to 5 mm/s. Coatings were obtained with two passes of the spray gun to form deposits of about 100 µm thickness. A temperature of working gas was varying parameter of: (1) 200 °C, (2) 400 °C and (3) 600 °C.

Characterization of Powders and Coatings

All produced samples were analyzed with surface visual assessment and using SEM (Hitachi S-3400 N, Tokyo, Japan) microscope equipped with SE, BSE detectors and EDS system for elemental analysis. The metallographic specimens were prepared by cutting the sample in the middle of its length. Afterward, the cross sections were polished without etching.

X-ray diffraction analyses were performed on the feedstock powders as well as on cold spray coated specimens to identify phases present on their surface. XRD measurements were carried out using Rigaku Ultima IV Diffractometer with Cu Kα irradiation (λ = 1.5406 Å) within the range from 10° to 60° in 0.02° steps with an exposure time of 4 s per point. Raman spectra were measured with Raman system (LabRAM HR800, HORIBA Jobin Yvon, 2007).

Thermogravimetric analysis and differential scanning calorimetry [DSC/TGA STA 449 F1 Jupiter instrument (Netzsch)] were performed on the TiO_2 feedstock powder at a heating rate of 5 K min^{-1}. Additionally, the same measurement on the powder detached from the coating produced with working gas preheated to 600 °C was conducted.

Results

Powder Characteristics

Scanning electron microscopy images of the TiO_2(am) feedstock powder obtained after the sol–gel synthesis and

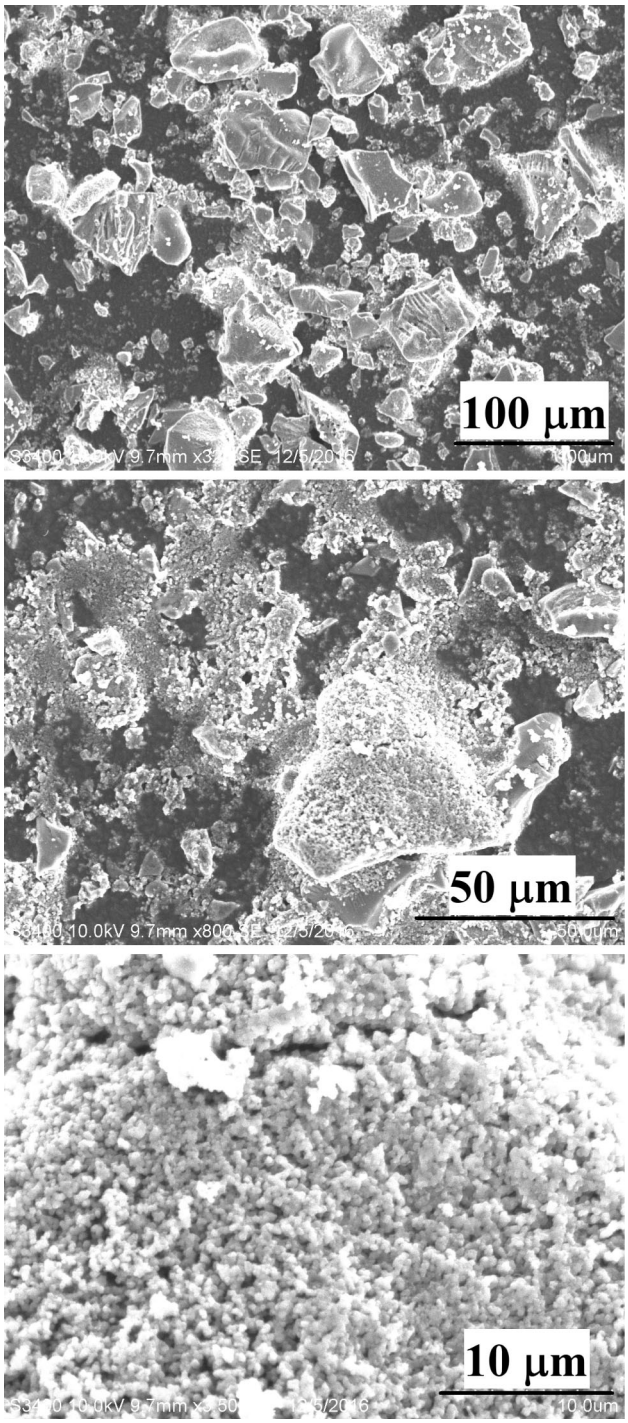

Fig. 1 Morphology of the TiO_2(am) powder after the sol–gel synthesis

dried in room temperature are displayed in Fig. 1. Analyzing SEM micrographs of as-synthesized amorphous TiO_2 powder, the strong agglomeration to structures of ~ 10-50 μm is clearly visible. These giant agglomerates are rather densely packed and consist of much smaller (~ 0.5 μm) regular and nearly spherical particles. The XRD diffraction pattern and Raman spectrum of the analyzed TiO_2(am) powder are shown in Fig. 2(a) and (b). The carried out measurements clearly demonstrate amorphous state of the feedstock material. The thermal behavior of TiO_2(am) powder was investigated with TG/DSC at temperatures ranging from room temperature to 750 °C. The TG/DSC patterns of the powder are shown in Fig. 3. Evidently, the weight loss proceeded in minimum three stages with increasing temperature, while the most significant weight loss occurred before ~ 400 °C. After ~ 400 °C, the thermogravimetric curve showed a nearly flat characteristic; thus, total weight loss was about 25%. Below 160 °C the weight loss is believed to result from the evaporation of water and the thermal decomposition of the remnant organic solvents such as isopropanol.

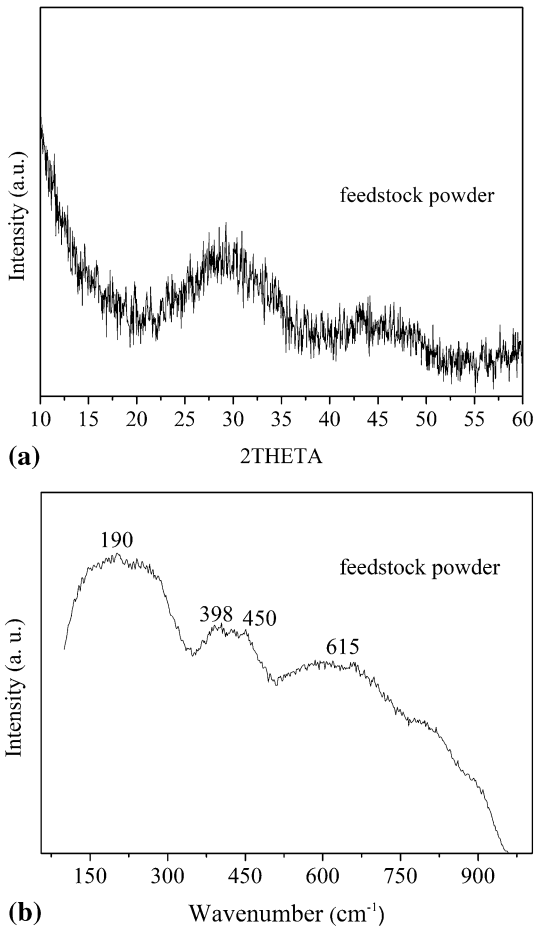

Fig. 2 XRD pattern (a) and Raman spectra (b) of the TiO_2(am) powder after the sol–gel synthesis

Between ~ 160 and ~ 260 °C the weight loss is attributed to the carbonization or the combustion of organic constituents in the sol precursor. Between 260 and 400 °C the weight loss is probably due to the evaporation of physically absorbed water and the further combustion of the remaining organic compounds (Ref 24). During the weight loss, two very broad endothermic peaks at around 100 and 250 °C are visible attributed to the loss of adsorbed water and decomposition of organic solvents. After the weight loss, there is a clear strong exothermic peak of crystallization between 400 and 463 °C (centered at 434 °C) in DSC curve of the amorphous powder indicating crystallization of the amorphous TiO_2 into anatase. A small exothermic peak centered at ~ 620 °C associated with the transformation from anatase to rutile is also visible.

Coatings Characteristics

The topographic morphologies of low-pressure cold-sprayed coatings with gas preheated to 200 °C are shown in Fig. 4(a) and (b). It is apparent that the coating demonstrates a rough surface morphology. Clearly, the humps visible on the surface were formed through the stacking of the deformed powder. The detailed examination of the surface morphology clearly showed that the surface structure (Fig. 4b) of the cold-sprayed coating was similar to that of the TiO_2(am) powder (Fig. 1c). The size of primary particles in the coating was observed to be ~ 0.5 μm, which is the same as that in the feedstock powder. The cross section of the cold-sprayed TiO_2 coating is shown in Fig. 4(c). It is clear that the coating demonstrates porous structure which was formed by rather loose stacking of primary amorphous particles. The XRD pattern of the coating sprayed with TiO_2(am) powder with gas preheated to 200 °C is presented in Fig. 5(a). The XRD pattern of the coating shows typical broad halos corresponding to

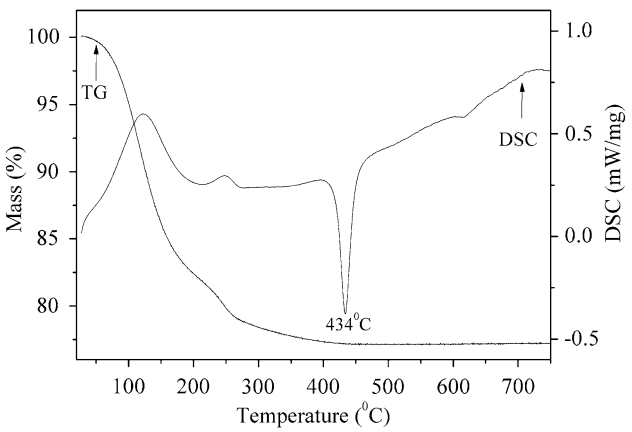

Fig. 3 TG–DSC curves of as-synthesized TiO_2 amorphous powder

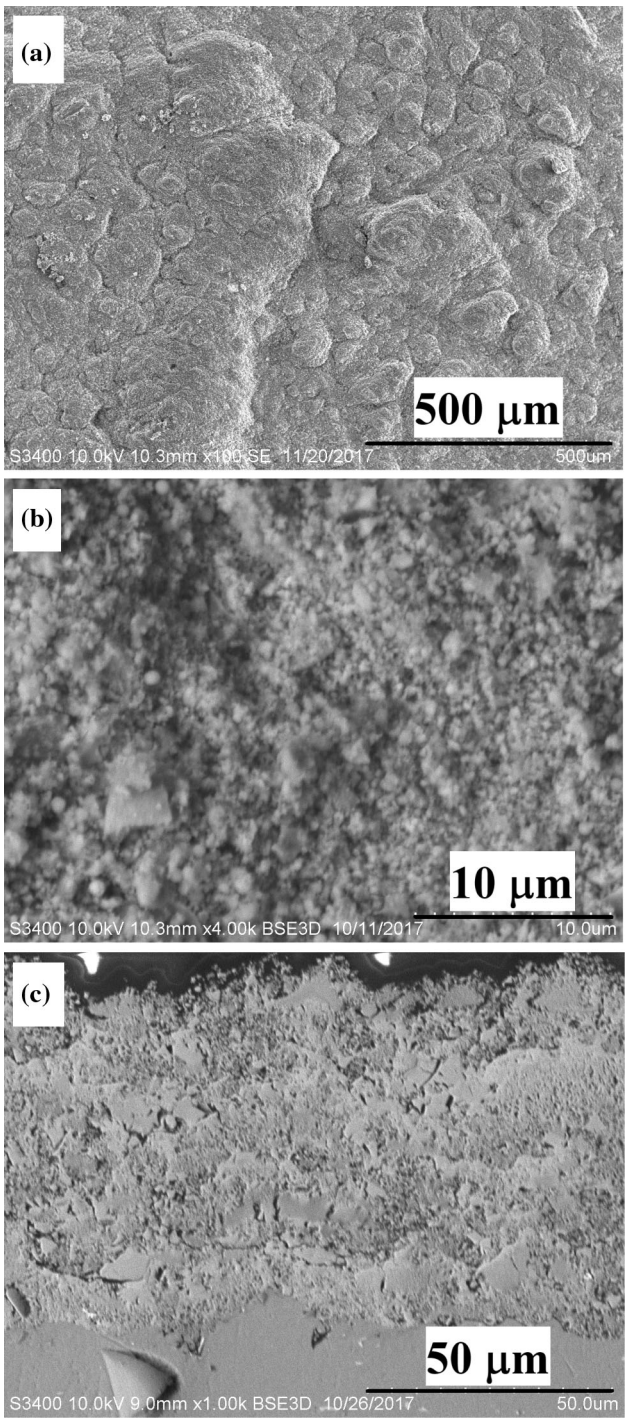

Fig. 4 Morphology of coating sprayed with TiO_2(am) feedstock powder with gas preheated to 200 °C surface (a, b), cross section (c) of the coating

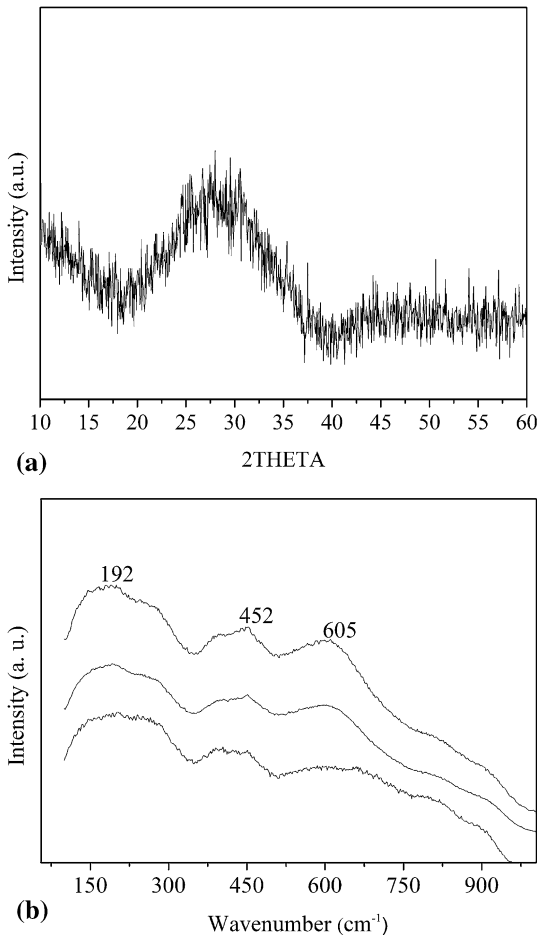

Fig. 5 Characteristics of the coating sprayed with TiO_2(am) feedstock powder with gas preheated to 200 °C: XRD pattern (a), Raman spectra measured at the three different locations on the coating surface (b)

amorphous structure which is confirmed by Raman spectra (Fig. 5b).

The surface of the coating sprayed with TiO_2(am) using gas preheated to 400 °C is shown in Fig. 6(a) and (b). It is evident that the coating demonstrates a rough surface morphology resembling morphology of the coating produced with gas preheated to 200 °C. The cross section of the coating is presented in Fig. 6(c). The detailed examination of the cross section morphology clearly showed two distinct types of stacked particles. In the upper part of the coating particles are less consolidated. Low packing density of TiO_2 particles in areas closest to the surface of the coating allows to distinguish primary particles with the same size as those in the feedstock powder. On the contrary, the consolidated particles in areas closest to the substrate demonstrate really high packing density. The shape of the starting particles could not be recognized in parts of image showing interface between coating and substrate. The XRD pattern of the coating sprayed with TiO_2(am) powder with gas preheated to 400 °C is shown in Fig. 7(a). Once again, the XRD pattern of the coating shows typical broad halos resulting from amorphous state of material. However, Raman spectra (Fig. 7b) reveal that amorphous titanium dioxide was partially transformed into crystalline anatase form during the process of spraying.

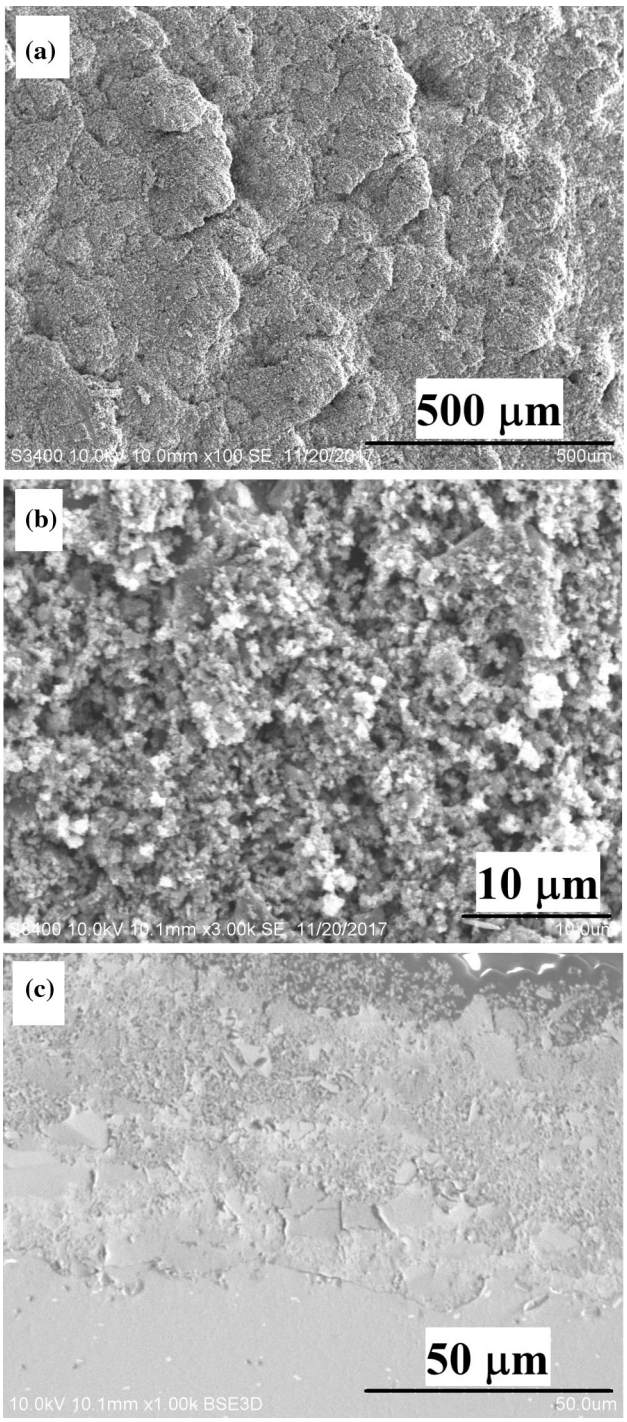

Fig. 6 Morphology of coating sprayed with TiO_2(am) feedstock powder with gas preheated to 400 °C: surface (a, b), cross section (c) of the coating

Depending on where on the coating surface the measurement was conducted, more or less sharp Raman peaks were visible. Precise analysis of Fig. 7(b) reveals peaks at 148 (E_g), 195 (E_g), 399 (B_{1g}), and 621 cm^{-1} (E_g), which can be assigned as modes reported for anatase.

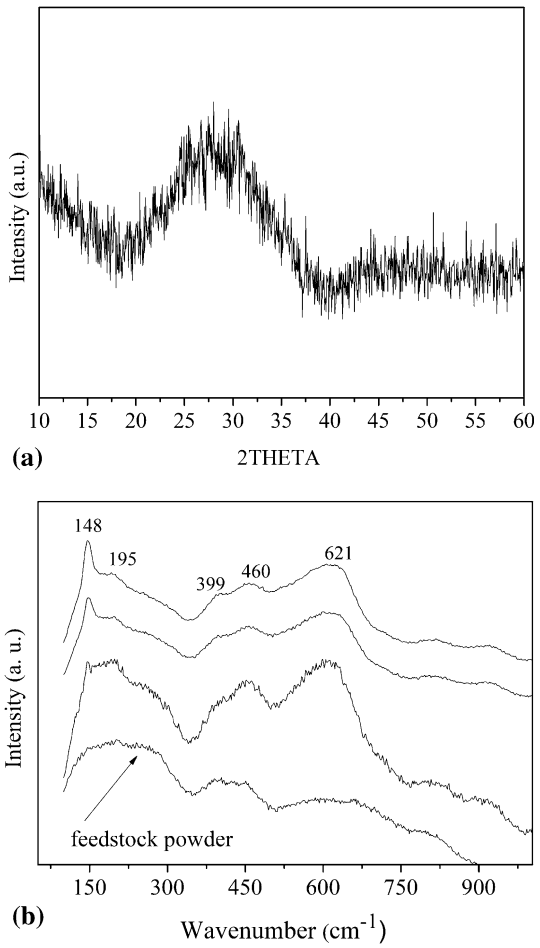

Fig. 7 Characteristics of the coating sprayed with TiO_2 amorphous feedstock powder with gas preheated to 400 °C: XRD pattern (a), Raman spectra measured at the three different locations on the coating surface (b). The spectrum of the feedstock powder was shown for comparison

The surface of coating sprayed with TiO_2(am) powder with gas preheated to 600 °C is presented in Fig. 8(a) and (b). Rough surface morphology does not deviate from those observed for coatings produced with gas preheated to lower temperatures. The detailed examination of the surface morphology clearly showed that apart from the same primary particles, as that in the feedstock powder $\sim$ 0.5 µm, also significantly bigger structures are observed. These structures look like crystalline grains and grain boundaries. The cross section of the low-pressure cold-sprayed TiO_2 coating is shown in Fig. 8(c). It is clear that the coating produced with gas preheated to 600 °C has the greatest thickness among coatings produced with lower gas temperatures. Moreover, higher density of the coating is also seen. Primary particles with the same size as that in the feedstock powder are observed only sporadically. The XRD pattern of the coating sprayed with amorphous TiO_2, with gas preheated to 600 °C is shown in Fig. 9(a). The

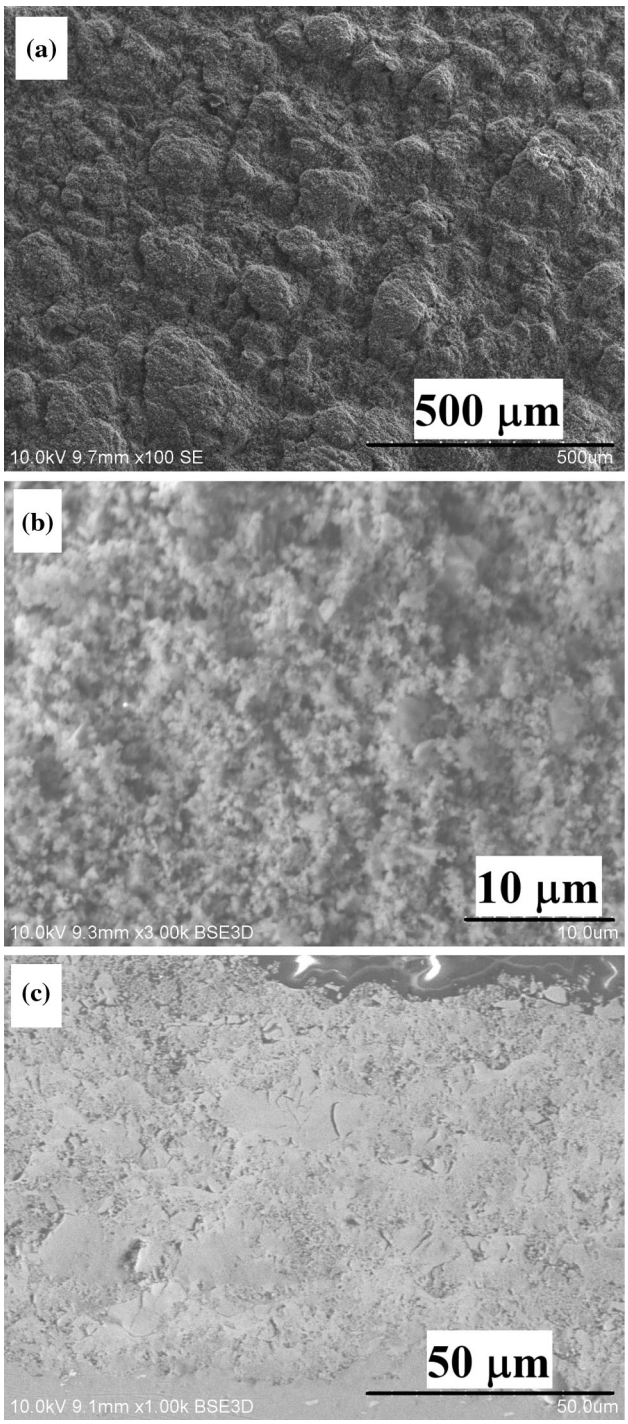

Fig. 8 Morphology of coating sprayed with TiO_2(am) feedstock powder with gas preheated to 600 °C: surface (a, b), cross section (c) of the coating

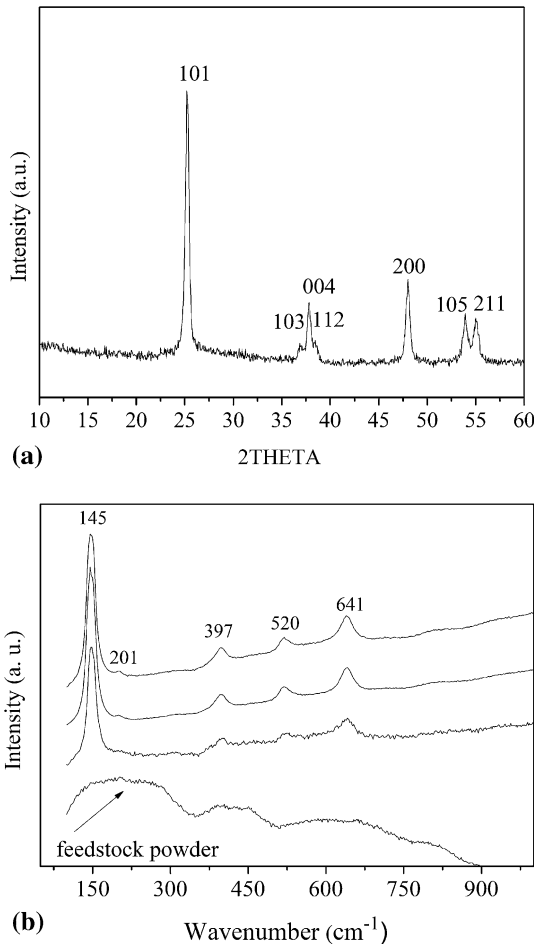

Fig. 9 Characteristics of the coating sprayed with TiO_2 amorphous feedstock powder with gas preheated to 600 °C: XRD pattern (a), Raman spectra measured at the three different locations on the coating surface (b). The spectrum of the feedstock powder was shown for comparison

XRD pattern of the coating shows seven typical distinctive peaks corresponding to anatase at 25.2° (101), 36.8° (103), 37.8° (004), 38.6° (112), 48° (200), 53.9° (105) and 55° (211). Raman spectra (Fig. 9b) clearly reveal that amorphous titanium dioxide was transformed into crystalline anatase form during the process of spraying. All Raman peaks shown in Fig. 9(b) can be assigned as the E_g (145 cm^{-1}), B_{1g} (201 cm^{-1}), A_{1g} (397 cm^{-1}), B_{1g} (520 cm^{-1}) and E_g (641 cm^{-1}) modes of the anatase phase. The thermal behavior of the powder obtained after the detachment of the coating from the substrate was investigated with TG/DSC at temperatures ranging from room temperature to 750 °C. The TG/DSC patterns obtained this way are shown in Fig. 10. Evidently, the weight loss takes place in stages with increasing temperature. The number of stages is lower than for TiO_2(am) powder. However, the most significant weight loss occurred before ~ 400 °C as in the case of TiO_2(am) gel. After ~ 400 °C the thermogravimetric curve showed a nearly flat characteristic. The total weight loss estimated from TG curve for powder recovered from the coating was about 8%, which is considerably less than 25% estimated for TiO_2(am) feedstock powder. During the weight loss, two peaks are visible. The first endothermic peak between 90 and 180 °C (centered

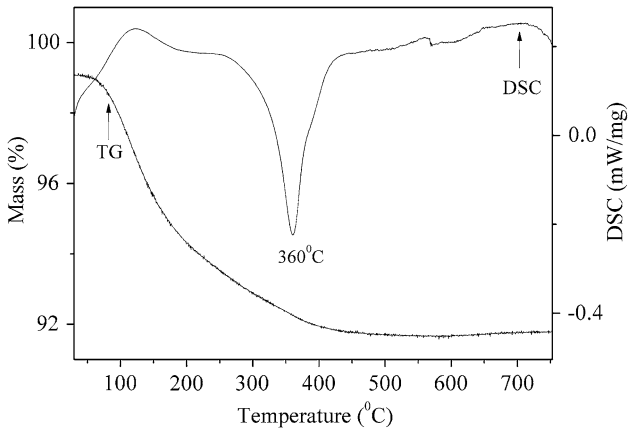

Fig. 10 TG–DSC curves of the powder detached from the coating produced with gas preheated to 600 °C

around 120 °C) can be linked mostly with the removal of water retained in partially dried powder and also with the desorption of organic residues that are still present in the sample (Ref 25). The second exothermic peak indicating crystallization of the amorphous TiO_2 into anatase is visible in DSC curve between 250 and 437 °C (centered at 360 °C).

Discussion

In the majority of papers showing the possibility of the thick ceramic coatings cold spraying, the agglomeration of the feedstock powder was recognized as being the most important factor for successful coatings fabrication (Ref 6-12). Analyzing SEM micrographs of as-synthesized amorphous sol–gel TiO_2 powder (see Fig. 1), strong agglomeration to structures of $\sim$ 10-50 μm is clearly visible. These giant agglomerates are rather densely packed and consist of much smaller ($\sim$ 0.5 μm) regular and nearly spherical particles. As it was shown in previous papers (Ref 8, 10), this close-packing agglomerated structure together with the minimized number of porosity is an important factor for successful ceramic powder cold spraying. It is obvious that the powder processing route has the main influence on the internal structure of the agglomerates and should be taken into an account. In this work sol–gel process was used in order to produce agglomerated TiO_2 powder. Liquid organic substances left after the sol–gel synthesis act as binders responsible for agglomeration. In this context, it may be accepted that analyzed here feedstock powder constitutes a form of soft agglomerates and can fracture easily during the impact, similarly as it was reported in (Ref 7-11). Primary analysis of the compactness of the cold-sprayed coatings from SEM micrographs (Fig. 4c, 6c, and 8c) revealed two distinct areas in coatings cross sections. It can be recognized easily that the upper and bottom part of the sections vary significantly in their compactness. It is clear that in areas closest to the substrate the consolidated particles demonstrate much higher packing density. Observed variation in coatings compactness can be explained by the tamping effect produced by continuous impact of incoming particles onto the substrate and onto the particles already adhered. When soft agglomerates are cold-sprayed, the high-speed collision onto a substrate causes shattering of the agglomerates into smaller particles. The porosity which is inherent to the agglomerates structure enables their deformation. The complete breakdown of agglomerates and scattering of fragments is, however, restricted due to above-mentioned liquid sol–gel process residues holding particles together.

On the basis of all these considerations, it can be stated that the mechanism of the coating formation, in case when TiO_2 gel is used as a feedstock, is similar as reported for other agglomerated non-sintered powders. However, it must not be forgotten that soft agglomerates used here consist of amorphous particles. In case of agglomerates constructed from the crystalline particles, plastic deformation mechanism takes place by slipping or sliding of particles over particles (Ref 11, 12). In case of analyzed here TiO_2 powder, this mechanism is also present. But amorphous state of the powder appears to be the additional factor responsible for cold spraying. The supplementary mechanism enabling effective powder deposition and coating production seems to be based on exotic for ceramic materials, plastic deformation. As it was mentioned in introduction, based on free volume theory, formation and propagation of shear bands are regarded as a common mechanism inducing plasticity in varieties of metallic and polymeric glasses as well as in amorphous oxides (Ref 17, 22, 23).

From the cross section images it can be seen that coatings areas closest to the substrate are characterized by relatively large, sharp-edged grains entirely distinct from the primary amorphous particles. This is a consequence of the conversion of kinetic energy into thermal energy. The local temperature rise is obviously high enough to induce crystallization of amorphous TiO_2. The process of crystallization seems to be initiated by the collision of particles onto the substrate, inducing shear deformation in ductile substrate material (Ref 28). Because the plastic deformation is localized at the particle–substrate interface, a significant temperature increase leading to anatase crystallization is observed in this region. However, the effectiveness of crystallization strongly increases as a result of subsequent particles impacting on pre-deposited crystalline TiO_2 grains, causing partial embedding of crystalline grains into metallic substrate. It should be noted that with increasing working gas temperature the area with

high packing density of TiO_2 particles considerably increases at the expense of area with low compactness. This is of course related to increasing transformation of amorphous titanium dioxide into crystalline anatase proven by XRD and Raman spectroscopy. Application of accelerating gas heated to 200 °C allows the relatively thick coating production, but it does not result in notable crystallization of TiO_2. Coatings deposited with gas preheated to 400 and 600 °C are thick, relatively dense and are characterized by significant level of crystallinity.

From the thermal analysis of the powder detached from the coating deposited with gas preheated to 600 °C (Fig. 10), it is clear that there is still significant amount of the amorphous phase present in the final coating. This is an observation of great importance because the possible existence of amorphous material in coating may reduce its photocatalytic activity (Ref 6, 8). Preliminary attempts to calculate the amount of amorphous phase have been ineffective due to the partial embedding of crystalline anatase grains into metallic substrate. Further, the primary hardness test results suggest that the coating surface was uneven which made it impossible to find the Vickers indentation marks to measure its hardness. Apparently, the coating deposited with gas preheated to 600 °C behaves mechanically as ceramic green body performs. This fact implies that nanoparticles in the coating are weakly bonded together. There is no doubt that post-sintering step causing welding between the particles can significantly improve hardness of the coating and should assist in the process of crystallization. On the other hand, calcination apart from increase in TiO_2 crystallinity may result in the formation of unfavorable rutile phase of TiO_2. Too high calcination temperature may also result in a considerable reduction of the coating active surface due to drastically increased crystalline size and consequently can have an adverse effect on photocatalytic performance (Ref 29). Hence, more detailed work reporting the optimum parameters for coatings post-treatments in terms of photocatalytic performance has been under preparation.

Since amorphous materials are not in thermodynamic equilibrium, phase transformation from amorphous to more stable crystalline phase can take place with the supply of external energy. Thermal annealing is typically used to produce thermally induced nanocrystallites that are homogeneously distributed in the amorphous matrix. The temperature of the process gas in this work undoubtedly influences crystallization process. It is obvious that the gas temperature has to be high enough to provide crystallization. However, it is enough to heat up accelerating gas to 400 °C in order to induce crystallization of TiO_2. Some might hold the view that this temperature is very close to the 434 °C, determined from DSC measurement as a temperature of the transformation from the amorphous gel to the crystalline anatase. It must, however, be remembered that determined from DCS crystallization temperature depends on the heating rate. It is obvious that heat transport from and to particles needs time. In DCS experiment TiO_2 particles were heated with the heating rate of 5 K min^{-1}, incomparably slower than heating rate typical in cold spraying. The residence time of particles in the hot gas stream is extremely short, and it can be assumed that is shorter than 1 μs (Ref 30). Furthermore, amorphous TiO_2 powder is introduced into the nozzle in its divergent part at the distance of 23.08 mm behind the throat. Thus, the temperature of the process gas at the time when it comes into contact with powder has to be significantly lower. It has been already shown based on numerical simulations for the same experimental conditions that this temperature is approximately 50% lower compared to temperature at the nozzle entrance, independently of the gas pressure (Ref 31).

Consequently, in the light of the considerations set out above it can be concluded that analyzed in this work transformation from the amorphous gel to the crystalline anatase cannot be only heat-induced. It must be stated that the increase in the temperature of the working gas could enhance the adiabatic shear instability zone in the ductile substrate and as a consequence lead to significant local temperature increase. Therefore, in the adiabatic shear instability region the temperature can reach the value necessary for crystallization. However, this phenomenon of the deformation-induced crystallization can arise not just from deformation of the ductile substrate but also from deformation of the amorphous oxide powder (Ref 32-35). For the first time significant nanocrystallization during deformation in amorphous mixture of Al_2O_3 and ZrO_2 (precisely:Al_2O_{3-x} mol.% ZrO_2 where x = 20, 40, 60, and 80) was reported in 2017 by Xu et al. (Ref 21). Authors observed that samples with 20 and 40% of ZrO_2 remain amorphous after deformation and exhibit brittle fracture. In the samples with 60 and 80% of ZrO_2 nanocrystallites of tetragonal-ZrO_2 were detected after significant plastic deformation. The same authors (Ref 21) demonstrated that the deformation-induced nanocrystallization in turn promoted the further significant plastic deformation due to the easier formation of shear bands at nanocrystallite/amorphous matrix interface. In recent years, plastic deformation improved by a second phase in the form of nanocrystallites was reported for the group of amorphous alloys (Ref 36-38). It is well known that plastic deformation of metallic glasses is entirely localized into thin shear bands. The simplest method in order to avoid the early failure of bulk metallic glasses upon loading is to add secondary phases which can directly hinder the evolution of shear bands into macrocracks and encourage the formation of multiple shear bands (Ref 38, 39). Despite current extensive

investigations, detailed mechanism describing enhanced plasticity of partially crystallized amorphous alloys with nanometer-sized crystals is still not clear. Much more research for the group of amorphous oxides is needed.

Conclusions

In this study the TiO_2 powder was successfully synthesized by sol–gel method without the addition of binder and/or inorganic salt. Then, this amorphous powder was used directly as a feedstock powder for low-pressure cold spraying without any post-treatment. The detailed SEM, Raman and XRD measurements clearly demonstrated that during the process of low-pressure cold spraying the amorphous titanium dioxide is transformed into crystalline anatase form. This transformation is accelerated by increasing temperature of the powder carrying gas. Application of accelerating gas heated to 600 °C allows to produce thick, relatively dense coatings characterized by significant level of crystallinity. This opens a new alternative route to produce nanocrystalline thick and dense TiO_2 coatings using the conventional cold spraying technique.

Acknowledgments The research was financed by the Department of Mechanics, Materials Science and Engineering, Wroclaw University of Science and Technology, under the Contract No. 0401/0029/17. Additional support was provided by Polish National Science Centre under the Contract No. 2016/23/D/ST8/00675 (Project title: The mechanism of joining submicron ceramic particles in cold spraying process).

References

1. K. Hashimoto, H. Irie, and A. Fujishima, TiO_2 Photocatalysis: A Historical Overview and Future Prospects, *Jpn. J. Appl. Phys.*, 2005, **44**(12R), p 8269-8285 (in English)
2. T. Watanabe, A. Nakajima, R. Wang, M. Minabe, S. Koizumi, A. Fujishima, and K. Hashimoto, Photocatalytic Activity and Photoinduced Hydrophilicity of Titanium Dioxide Coated Glass, *Thin Solid Films*, 1999, **351**(1), p 260-263 (in English)
3. Y. Jiang, P. Zhang, Z. Liu, and F. Xu, The Preparation of Porous Nano-TiO_2 with High Activity and the Discussion of the Cooperation Photocatalysis Mechanism, *Mater. Chem. Phys.*, 2006, **99**(2), p 498-504 (in English)
4. M.P. Fedotova, G.A. Voronova, E.Y. Emel'yanova, N.I. Radishevskaya, and O.V. Vodyankina, Nanodisperse Photocatalysts Based on Titanium Dioxide, *Russ. J. Phys. Chem. A*, 2009, **83**(8), p 1371-1375 (in nglish)
5. A. Wold, Photocatalytic Properties of Titanium Dioxide (TiO_2), *Chem. Mater.*, 1993, **5**(3), p 280-283 (in English)
6. M. Gardon and J.M. Guilemany, Milestones in Functional Titanium Dioxide Thermal Spray Coatings: A Review, *J. Therm. Spray Technol.*, 2014, **23**(4), p 577-595 (in English)
7. G.J. Yang, C.J. Li, F. Han, W.Y. Li, and A. Ohmori, Low Temperature Deposition and Characterization of TiO_2 Photocatalytic Film Through Cold Spray, *Appl. Surf. Sci.*, 2008, **254**(13), p 3979-3982 (in English)
8. A.R. Toibah, M. Sato, M. Yamada, and M. Fukumoto, Cold-Sprayed TiO_2 Coatings from Nanostructured Ceramic Agglomerated Powders, *Mater. and Manuf.*, 2016, **31**(11), p 1527-1534 (in English)
9. T.A. Rahim, K. Takahashi, M. Yamada, and M. Fukumoto, Effect of Powder Calcination on the Cold Spray Titanium Dioxide Coating, *Mater. Trans.*, 2016, **57**(8), p 1345-1350 (in English)
10. N.T. Salim, M. Yamada, H. Nakano, K. Shima, H. Isago, and M. Fukumoto, The Effect of Post-Treatments on the Powder Morphology of Titanium Dioxide (TiO_2) Powders Synthesized for Cold Spray, *Surf. Coat. Technol.*, 2011, **206**(2-3), p 366-371 (in English)
11. A.M. Vilardell, N. Cinca, I.G. Cano, A. Concustell, S. Dosta, J.M. Guilemany, S. Estradé, A. Ruiz-Caridad, and F. Peiró, Dense Nanostructured Calcium Phosphate Coating on Titanium by Cold Spray, *J. Eur. Ceram. Soc.*, 2017, **37**(4), p 1747-1755 (in English)
12. N. Cinca, A.M. Vilardell, S. Dosta, A. Concustell, I. Garcia Cano, J.M. Guilemany, S. Estradé, A. Ruiz, and F. Peiró, A New Alternative for Obtaining Nanocrystalline Bioactive Coatings: Study of Hydroxyapatite Deposition Mechanisms by Cold Gas Spraying, *J. Eur. Ceram. Soc.*, 2016, **99**(4), p 1420-1428 (in English)
13. D. Hanft, J. Exner, M. Schubert, T. Stöcker, P. Fuierer, and R. Moos, An Overview of the Aerosol Deposition Method: Process Fundamentals and New Trends in Materials Applications, *J. Ceram. Sci. Technol*, 2015, **6**(3), p 147-182 (in English)
14. A.S. Gandhi and V. Jayaram, Plastically Deforming Amorphous ZrO_2–Al_2O_3, *Acta Mater.*, 2003, **51**(6), p 1641-1649 (in English)
15. A. Paul and V. Jayaram, Deformation and Structural Densification in Al_2O_3–Y_2O_3 Glass, *Acta Mater.*, 2011, **59**(1), p 82-92 (in English)
16. X. Xu, Y. Wang, A. Guo, H. Geng, S. Ren, X. Tao, and J. Liu, Enhanced Plasticity by Nanocrystallite in Bulk Amorphous Al_2O_3–ZrO_2–Y_2O_3, *Int. J. Plast*, 2016, **79**, p 314-327 (in English)
17. X. Xu, A. Guo, Z. Gong, H. Du, F. Hou, and J. Liu, Evaluation of Metastable Degree in Amorphous Al_2O_3–ZrO_2–Y_2O_3 and Its Effect on Plastic Deformation, *J. Alloys Compd.*, 2017, **701**, p 645-651 (in English)
18. X. Xu, X. Xu, J. Liu, W. Hong, H. Du, and F. Hou, Low-Temperature Fabrication of Al_2O_3–ZrO_2 (Y_2O_3) Nanocomposites Through Hot Pressing of Amorphous Powders, *Ceram. Int.*, 2016, **42**(13), p 15065-15071 (in English)
19. Y. Wang, J. Liu, and A. Guo, Moderate Temperature Compression Incorporating Plastic Deformation and Rearrangement in Al_2O_3–ZrO_2 Ceramics, *Ceram. Int.*, 2013, **39**(1), p 883-886 (in English)
20. X. Xu, M. Wang, A. Guo, X. Tao, X. Hu, and J. Liu, Plastic Deformation Promoted by Phases Separation in Bulk Amorphous Al_2O_3–ZrO_2–Y_2O_3, *Mater. Lett.*, 2016, **170**, p 15-17 (in English)
21. X. Xu, C. Zhai, H. Ren, L. Guo, F. Hou, and J. Liu, Enhanced Plasticity by Deformation-Induced Nanocrysallization in Bulk Amorphous Al_2O_3–ZrO_2–Y_2O_3, *Ceram. Int.*, 2017, **43**(3), p 3453-3456 (in English)
22. G.N. Yang, B.A. Sun, S.Q. Chen, Y. Shao, and K.F. Yao, The Multiple Shear Bands and Plasticity in Metallic Glasses: A Possible Origin from Stress Redistribution, *J. Alloys Compd.*, 2017, **695**, p 3457-3466 (in English)

23. V. Jatin and S. Sudarkodi, Basu, Investigations into the Origins of Plastic Flow and Strain Hardening in Amorphous Glassy Polymers, *Int. J. Plast*, 2014, **56**, p 139-155 (in English)
24. C. Legrand-Buscema, C. Malibert, and S. Bach, Elaboration and Characterization of Thin Films of TiO_2 Prepared by Sol–Gel Process, *Thin Solid Films*, 2002, **418**, p 79-84 (in English)
25. D. Švadlák, J. Shánělová, J. Málek, L.A. Pérez-Maqueda, J.M. Criado, and T. Mitsuhashi, Nanocrystallization of Anatase in Amorphous TiO_2, *Thermochim. Acta*, 2004, **414**(2), p 137-143 (in English)
26. M. Guglielmi, Sol–gel Coatings on Metals, *J. Sol Gel. Sci. Technol.*, 1997, **8**(1–3), p 443-449 (in English)
27. A. Baszczuk, M. Jasiorski, B. Borak, and J. Wodka, Insights into the Multistep Transformation of Titanate Nanotubes into Nanowires and Nanoribbons, *Mater. Sci. Pol.*, 2016, **34**(4), p 691-702 (in English)
28. J.O. Kliemann, H. Gutzmann, F. Gartner, H. Hubner, C. Borchers, and T. Klassen, Formation of Cold-Sprayed Ceramic Titanium Dioxide Layers on Metal Surfaces, *J. Therm. Spray Technol.*, 2011, **20**(1–2), p 292-298 (in English)
29. J.I. Garza-Arévalo, I. García-Montes, M.H. Reyes, J.L. Guzmán-Mar, V. Rodríguez-González, and L.H. Reyes, Fe Doped TiO_2 Photocatalyst for the Removal of As(III) Under Visible Radiation and Its Potential Application on the Treatment of As-Contaminated Groundwater, *Mater. Res. Bull.*, 2016, **73**, p 145-152 (in English)
30. V. Champagne, *The Cold Spray Materials Deposition Process: Fundamentals and Applications*, Woodhead Publishing Ltd., Cambridge, 2007
31. M. Winnicki, A. Małachowska, G. Dudzika, M. Rutkowska-Gorczyca, M. Marciniaka, K. Abramskia, A. Ambroziak, and L. Pawłowski, Numerical and Experimental Analysis of Copper Particles Velocity in Low-Pressure Cold Spraying Process, *Surf. Coat. Technol.*, 2015, **268**, p 230-240 (in English)
32. R.J. Hebert, J.H. Perepezko, H. Rösner, and G. Wilde, Dislocation Formation During Deformation-Induced Synthesis of Nanocrystals in Amorphous and Partially Crystalline Amorphous Al88Y7Fe5 Alloy, *Scr. Mater.*, 2006, **54**(1), p 25-29 (in English)
33. N. Boucharat, R. Hebert, H. Rösner, R. Valiev, and G. Wilde, Nanocrystallization of Amorphous Al88Y7Fe5 Alloy Induced by Plastic Deformation, *Scr. Mater.*, 2005, **53**(7), p 823-828 (in English)
34. Z. Kovács, P. Henits, A.P. Zhilyaev, and Á. Révész, Deformation Induced Primary Crystallization in a Thermally Non-primary Crystallizing Amorphous Al85Ce8Ni5Co2 Alloy, *Scr. Mater.*, 2006, **54**(10), p 1733-1737 (in English)
35. Á. Révész, S. Hóbor, P.J. Szabó, A.P. Zhilyaev, and Z. Kovács, Deformation Induced Crystallization in an Amorphous Cu60Zr20Ti20 Alloy by High Pressure Torsion, *Mater. Sci. Eng. A*, 2007, **460**, p 459-463 (in English)
36. S.W. Lee, M.Y. Huh, S.W. Chae, and J.C. Lee, Mechanism of the Deformation-Induced Nanocrystallization in a Cu-Based Bulk Amorphous Alloy Under Uniaxial Compression, *Scr. Mater.*, 2006, **54**(8), p 1439-1444 (in English)
37. W.H. Jiang, F.E. Pinkerton, and M. Atzmon, Deformation-Induced Nanocrystallization in an Al-Based Amorphous Alloy at a Subambient Temperature, *Scr. Mater.*, 2003, **48**(8), p 1195-1200 (in English)
38. H. Zhou, S. Qu, and W. Yang, An Atomistic Investigation of Structural Evolution in Metallic Glass Matrix Composites, *Int. J. Plast.*, 2013, **44**, p 147-160 (in English)
39. J. Qiao, H. Jia, and P.K. Liaw, Metallic Glass Matrix Composites, *Mater. Sci. Eng. R*, 2016, **100**, p 1-69 (in English)